ELSEVIER

Journal of Hydrology 200 (1997) 84–109

Journal of Hydrology

Runoff generation processes estimated from hydrological observations on a steep forested hillslope with a thin soil layer

Makoto Tani

Forestry and Forest Products Research Institute, P.O. Box 16, Tsukuba Nourin Kenkyuu Danchi-Nai, Ibaraki, 305 Japan

Received 13 August 1996; accepted 17 December 1996

Abstract

In order to understand runoff generation processes on a forested hillslope involving large heterogeneities, this study monitored runoff from a steep hillslope with a thin soil layer as well as matric potential within it and analyzed their responses to storm rainfall. A comparison of storm runoff responses from the study slope with those from two adjacent catchments, one of which includes it, showed that physical properties of the slope reflected the runoff characteristics: although no responses occurred in very dry conditions because of the absence of wet zones near the stream, the area contributing to storm runoff more rapidly extended to the whole slope due to its topographic properties. They also caused its steep hydrographs produced in the wettest condition where almost all the rainfall contributed to storm runoff. In this wettest condition, tensiometric responses near bedrock showed the vertical quick propagation of the rainfall pulse, and a good agreement of storm hydrograph simulated through a kinematic wave runoff model suggested that runoff from the slope was produced by a lateral flow on the bedrock receiving the quick propagation. In a transition process from dry to the wettest conditions, the development of the lateral flow producing smaller responses at the downslope end was estimated from decreasing of matric potential near bedrock from high negative to low values with increasing cumulative rainfall. © 1997 Elsevier Science B.V.

Keywords: Runoff generation processes; Steep hillslope; Thin soil layer; Storm rainfall

1. Introduction

Generally rainwater falling onto the forest floor infiltrates into the hillslope soil (Kirkby, 1978). Thus, storm runoff is usually not produced by overland flow, and subsurface flow dominates. It has been debated whether a stormflow is directly discharged as the subsurface flow (Hewlett and Hibbert, 1963) or by saturated overland flow induced by the

PII S0022-1694(97)00018-8

subsurface flow exfiltrating near stream channels (Dunne and Black, 1970). However, hydrochemical studies have demonstrated that a stormflow is mainly composed of displaced 'old' water and a direct contribution of subsurface flow must be the dominant mechanism (e.g. Sklash et al., 1986).

The large water yields observed in some catchments (Mosley, 1979, 1987a) indicate that storm runoff generation is not limited to near the stream (Sklash and Farvolden, 1979) but comprises an expanded area within the catchment (Sidle et al., 1995). McDonnell (1990) emphasized the contribution of macropores to storm runoff and showed that both infiltration via soil cracks (bypass flow) and lateral pipe flow contribute significantly to storm runoff generation. He pointed out the importance of the displacement process of new event water by old water retained within the soil matrix to account for a large occupation of old water in runoff discharged through macropores.

The complex function of macropores raises problems for understanding hydrologic effects of soil physical properties at larger scales (i.e. hillslope scale and catchment scale) since simple physical laws such as the Richards equation should be applied only for homogeneous porous media. Once a heterogeneity is considered, it becomes difficult to explain hydrological responses based on these physical laws. Physical laws for the heterogeneities have not been established although properties of macropores at a field plot scale (not a slope scale) have been conducted (Mosley, 1979; Kitahara, 1993; Tsuboyama et al., 1994).

To consider the roles of macropores at larger scales, one strategy may be to evaluate the responses of runoff to storm rainfall. Information included in such responses may sometimes be underevaluated because observed hydrographs can easily be simulated by various types of runoff models (Betson, 1978). It is true that a good agreement between observed and simulated hydrographs itself does not validate model assumptions. However, such responses still give us the most important information on integrative runoff processes at a hillslope scale especially when they are analyzed with results from detailed field observations at a point scale such as tensiometric responses.

Runoff models suitable for such analyses may be somewhat different from models for homogeneous soils based on the Richards equation (Freeze, 1971). They would not address the detailed physics within the soil matrix but instead reflect rapid downslope flows affected by uncertain heterogeneities at a hillslope scale. A simple kinematic wave runoff model has often been applied to runoff analyses for rapid downslope flow within soil on hillslopes (Beven, 1981; Sloan and Moore, 1984; Kubota and Sivapalan, 1995) although this originally assumed overland flow described by the Manning equation (Ishihara and Takasao, 1963). This model may be applied for the rapid downslope flow through pathways with heterogeneities.

Considering these backgrounds, we attempt to analyze runoff and tensiometric responses using a runoff model to understand runoff generation processes on a hillslope. First, general runoff characteristics of the entire catchments, one of which includes the study hillslope, will be investigated. The most important information is that almost all the rainfall contributes to storm runoff when the soil condition is the wettest. This will be used as a clue for both a quantitative evaluation of drainage area for the study slope and an estimation of flow pathways in it by the model application. General runoff generation processes in a transition from dry to the wettest conditions will be discussed based on findings in the wettest condition.

2. Site description

2.1. Entire catchments

The study was conducted in the Tatsunokuchi-yama Experimental Forest (34°42′N, 133°58′E) of the Forestry and Forest Products Research Institute (FFPRI) located on a hilly mountain near Okayama City in Japan (Fig. 1). Effects of forest changes on streamflow have been studied in two adjacent catchments, Minamitani (MN) and Kitatani (KT), for more than 58 years since 1937 (Nakano, 1967; Fujieda and Abe, 1982). Runoff from each of the catchments has been monitored at a 60° V-notch gauging weir and precipitation and other climatic factors have been measured at an observation station.

Average values of annual precipitation, annual potential evaporation measured by a 20-cm pan, and annual mean temperature are 1228.7 mm, 1050 mm, and 14.3°C, respectively. Seasonal fluctuations of these climatic factors (Fujieda and Abe, 1982) show two peaks of monthly precipitation in June and September with a very dry summer between them.

The catchment areas of KT and MN are 17.27 ha and 22.61 ha, respectively. The average slope length and gradient are 121 m and 23.8° for MN and 123 m and 28.4° for KT, respectively. Although the catchments are mainly underlain with Paleozoic formations, portions of steeper slopes in both catchments are underlain with quartz porphyry. Quartz porphyry underlies 6% of MN with an average slope length and gradient of 57 m and 31.0°, whereas 35% of KT contains quartz porphyry with an average slope length and gradient of 104 m and 31.1°. Thin organic soil (5–10 cm) is underlain by deep immature mineral soil of stony clay loam. An electrical resistivity survey showed the depth of bedrock to be about 5 m (Kidachi et al., 1977). The thickness of the mineral soil tends to be much smaller in the areas of quartz porphyry than in those of Paleozoic formations.

Vegetation in the MN catchment changed several times during the history of hydrological experiment since 1937. After forest fire occurred in the whole MN area in 1959, Japanese black pine trees (*Pinus thumbergii*) were planted. The pine trees were killed completely by the pine-wood nematode in 1980 (Abe and Tani, 1985; Tani and Abe, 1987b). Deciduous and evergreen broad-leaved trees (*Quercus serrata*, *Eurya japonica*, *Ilex predunculosa*, etc.) which had underlain the canopies of pine tree succeeded them after the killing and covered the MN catchment in the main period of our present study in the 1980s. Vegetation in the KT catchment was a natural mixed forest of deciduous and evergreen trees (similar species to MN) which succeeded after the clearcutting of an old Japanese red pine forest (*Pinus densiflora*) in the 1940s (Nakano, 1967). This vegetation continued until the main study period.

2.2. Study slope

Slope runoff was monitored in a 6-m trench (width = 0.5 m) that was constructed in March 1986 on exposed bedrock at the bottom of a hillslope along the stream channel in the MN catchment (Fig. 1). The length and average gradient of this study slope (SL) are 42.7 m and 34.6°. A fence (height = 0.4 m) made of concrete blocks was fixed with mortar

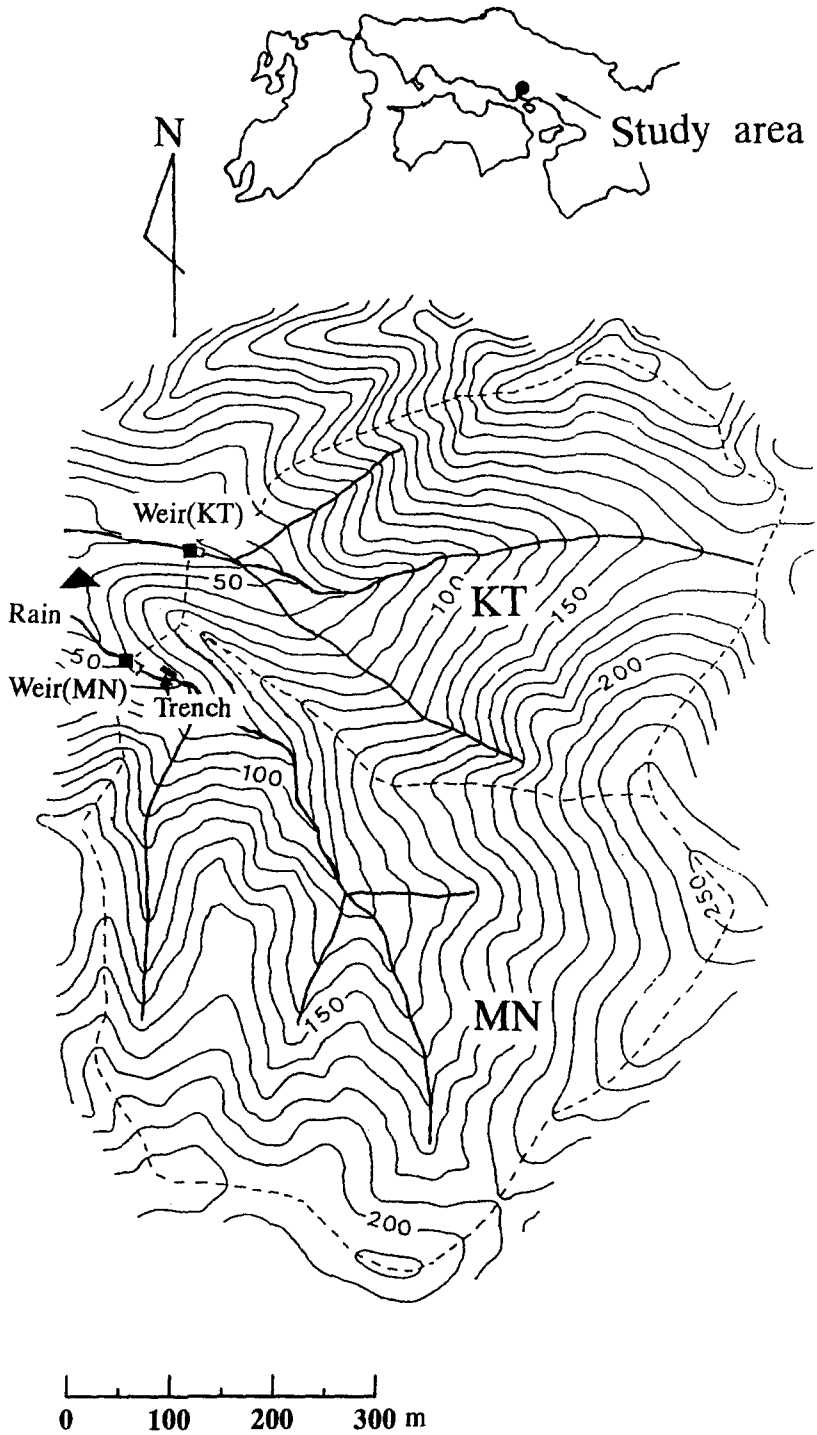

Fig. 1. Location map of Minamitani catchment (MN), Kitatani catchment and the trench of the study slope (SL) in the Tatsunokuchi-yama Experimental Forest.

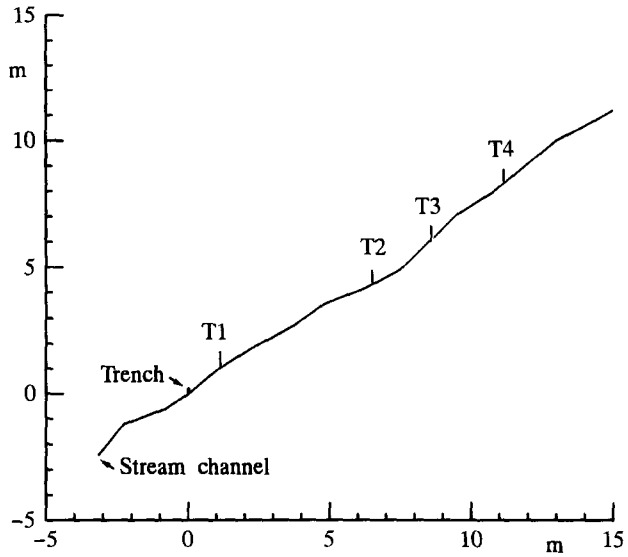

Fig. 2. Location of tensiometer sites on the longitudinal profile of the study slope (SL).

to the bedrock to stop any leakage across the fence. Runoff water intercepted by the fence was routed into a 60° V-notch weir. The outlet from the weir was monitored by a flow meter with a 1-l tipping bucket to obtain accurate data for small flows.

The SL is shorter and steeper than average slopes in MN. The geology at the runoff study site is quartz porphyry. Mineral soil is very thin compared with other areas of MN and the total depth including organic soil (the thickness of about 5 cm) is usually around 50 cm. An old landslide was found halfway up the slope and bedrock was exposed at the head wall of the landslide. Observations of soil profile at the trench showed that the mineral soil contained many macropores which produced much runoff discharge preferentially during storm events. The values of saturated hydraulic conductivity for two samples of mineral soil (surface area 100 cm^2; the thickness of 4 cm) collected at the 15-cm depth on the lower part of the slope are 1.7 and 6.3×10^{-3} cm s^{-1} based on the constant-head method. Soil textures are clay loam and sandy loam for these samples. The natural broad-leaved forest on this slope was in poor condition compared with other areas of the MN catchment.

Matric potential in soil was monitored at four sites on the downslope portion of the study slope by an automatic tensiometer system. Fig. 2 shows the locations of tensiometer sites. Because bedrock occurs at about 50 cm depth, at least one porous cup was installed just near the bedrock for four sites (T1 to T4). The depths for T1, T2, T3, and T4 were 46, 40, 40, and 50 cm, respectively. Additional cups were installed at 10 cm for T1 and at 10 cm and 30 cm for T4 to estimate the transmission process of potential. Rough relationships of matric potential to mass-basis water content were investigated, sometimes collecting disturbed soil samples (the weight of several grams) by a bore stick at T1 and T4.

3. Hydrological characteristics of the catchments

3.1. Total storm rainfall and runoff relationships

Runoff responses for catchments MN and KT have been investigated, using the long-term hydrologic data. Tani and Abe (1987a) showed that ratios of total storm runoff to total rainfall in catchment KT were generally related to the storm magnitude and the antecedent water storage in the catchment. The storm runoff volume was calculated by simple hydrograph separation with a straight line connected from the point of initial runoff to the inflection point on the recession limb on a semi-logarithmic graph scale. The inflection time was picked up considering an empirical relationship between the termination time of storm runoff and the catchment area (Linsley et al., 1949). Initial runoff rate (Q_i) just before hydrograph rising due to storm rainfall was used as an indicator for the antecedent soil water condition averaged over the whole catchment. Storm runoff was less than 10% of rainfall if antecedent conditions were dry and the rainfall did not exceed 100 mm. When total rainfall was greater than 100 mm, the increase in storm runoff was almost equal to the increase in rainfall, even with dry antecedent conditions. For wetter antecedent conditions, less cumulated rainfall was required before the increase in storm runoff approached that in rainfall. The relations at MN were similar to those at KT, although the volumes of runoff at MN tended to be a little smaller than at KT (Tani et al., 1982). Thus, we can conclude that almost all the rainfall contributes to storm runoff in both catchments when the soil condition is the wettest.

3.2. Kinematic wave runoff model and its previous application

A kinematic wave runoff model has often been used for storm runoff predictions (Ishihara and Takasao, 1963; Beven, 1981). The equations of this model are written as

$$S = kQ^p \tag{1}$$

$$\frac{\partial S}{\partial T} + \frac{\partial Q}{\partial x} = i \tag{2}$$

where S is the total water volume of downslope flow per unit length and unit width, Q is the lateral flow rate per unit width, p and k are empirical parameters, i is the effective rainfall intensity, that is, the rate of water input to the lateral flow per unit length and unit width, t is time, and x is the distance downslope.

Tani and Abe (1987a) applied this model to simulate a storm runoff response at KT including the occurrence of several runoff peaks. The simulation was carried out for the average slope (horizontal length = 123 m; slope angle = 28.4°) in the KT catchment and the simulated hydrograph was compared with that observed for the entire catchment in Fig. 3. During the storm event (8–13 September 1976), the initial dry condition gradually became very wet due to 372.2 mm of cumulative rainfall. The observed volumes of rainfall and storm runoff were almost the same during the latter half of the storm. For the wettest condition, i was simply estimated as $r \cos \omega$ from the observed rainfall r and the slope

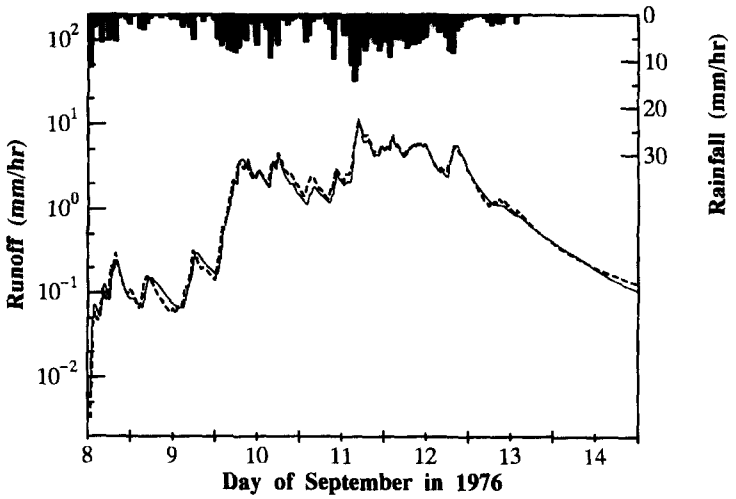

Fig. 3. Comparison between observed and simulated hydrographs responding to a big storm event of 8–13 September 1976 for KT catchment. —, Observed; - - - -, simulated.

angle ω. Values of the two parameters, p and k, were optimized as 0.3 and 0.6 $m^{0.4}$ $s^{0.3}$, from the hydrograph during the wettest period.

In the early dry stage of the event, several small responses were simulated by using the optimized parameters with an additional assumption about the effective rainfall given to the lateral flow. The assumption was that no effective rainfall was given to it until cumulative rainfall reached an initial threshold which would increase upslope and that all rainfall on the area where cumulated rainfall had exceeded the threshold would be given as effective rainfall to the lateral flow. The assumed distribution of initial threshold was based on the estimation that soil water deficit would become large upslope away from the stream channel. Fig. 3 shows one of the best results for the distribution of initial threshold soil water deficit given empirically in Fig. 4. The simulated hydrograph agreed with observations made during both the early dry stage as well as in the later wet stage. For the dry condition, a runoff response was very small but fast. These characteristics in the

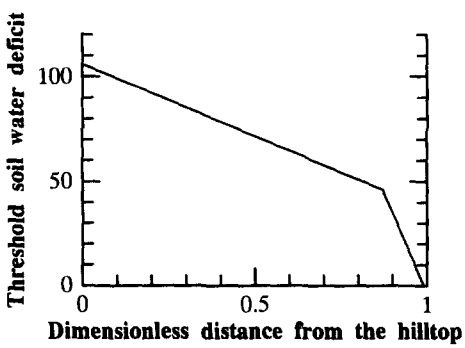

Fig. 4. The distribution of initial threshold soil water deficit just before the storm event of 8–13 September 1976 empirically estimated for average slope of KT catchment.

observed hydrograph could be understood based on the model assumption that the lateral flow was generated only from downslope portions of the slope. The initial threshold soil water deficit in Fig. 4 first increased rapidly with increasing distance from channel, and then gradually increased in the upslope area. A similar distribution of soil water deficit was obtained from a topographic analysis of Crimple Beck catchment in the United Kingdom (Beven and Wood, 1983). However, the distribution was obtained not from a field investigation but from a comparison of a simulated hydrograph with that observed. Further studies are necessary for runoff generation in dry conditions.

Thus, we have faced basic subjects to be investigated: (1) although the model applied to a single averaged slope, we have compared the simulated hydrograph to that obtained not from the slope but from a catchment consisting of stream channels and many slopes with different runoff characteristics; (2) no physical background exists for defining effective rainfall from rainfall observed or for identifying pathways of lateral stormflow. These points strongly require runoff data observed at a unit slope as well as data for temporal and spatial distributions of soil water. The following analyses in the present paper will incorporate results from both runoff and matric potential in the study slope to understand runoff generation processes of a single slope.

4. Runoff responses

4.1. Total storm rainfall and runoff relationships

Relationships of the total storm rainfall and runoff for our study slope (SL) are compared with those of the whole MN catchment. Data from January in 1986 to November in 1987 were used in this investigation. A hydrograph separation procedure calculating storm runoff from total runoff (see Section 3.1) was first applied to MN and duration obtained for

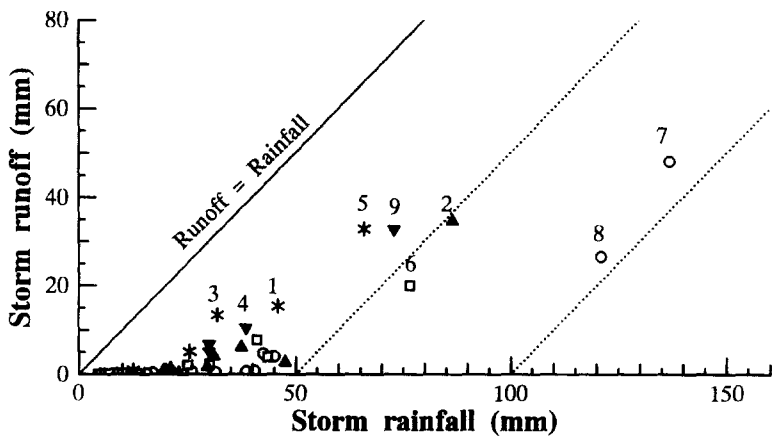

Fig. 5. Total storm rainfall and runoff relationships for catchment MN. ○, $Q_i \leq 0.005$ mm h^{-1}; □, $0.005 < Q_i \leq 0.0075$ mm h^{-1}; ▲, $0.0075 < Q_i \leq 0.01$ mm h^{-1}; ▼, $0.01 < Q_i \leq 0.02$ mm h^{-1}; *, $Q_i > 0.02$ mm h^{-1} where Q_i is the initial runoff rate of MN.

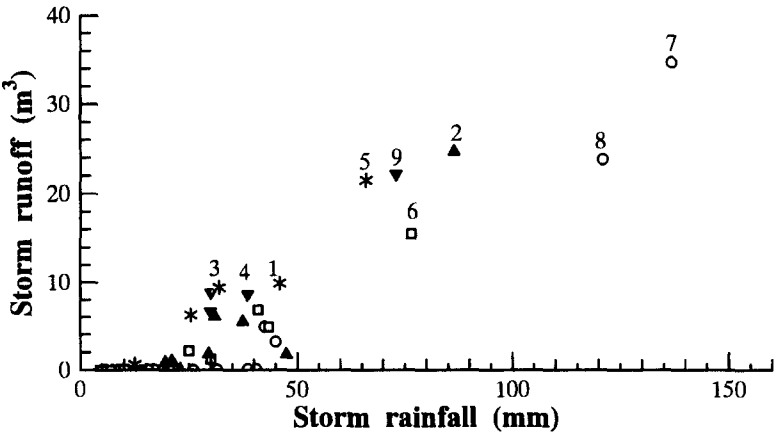

Fig. 6. Total storm rainfall and runoff relationships for slope SL. Symbols and storm numbers are the same as Fig. 5.

MN was then used for the hydrograph separation for SL. Figs. 5 and 6 show the relations of total runoff to total storm rainfall for MN and SL, respectively. Runoff from MN is expressed as average water depth (mm) over the entire catchment area, whereas runoff from SL is expressed as a volume (m^3). Since SL is situated on a linear slope, the area can be calculated as 245 m^2 from the width (6 m) and the horizontal length (42.7 m) of the slope, however, estimating a catchment area for such a small slope based on topography could be dubious. A more plausible catchment area for SL will be defined in Section 4.2.

Although the area has not been fixed for SL, some findings can be recognized from Figs. 5 and 6. Total runoff is quite small when total rainfall is less than 20 mm both for MN and SL. When the rainfall exceeds this value, storm runoff increases with rainfall. The increase depends strongly on the initial runoff rate (Q_i). This indicates that antecedent moisture conditions influence storm runoff responses in SL as well as in the entire catchments MN and KT as described in Section 3.1. Plots for large storm events (identified by numbers in Fig. 5) with similar values of Q_i (1, 3, and 5; 4 and 9; 7 and 8) tend to be parallel to the line of runoff = rainfall. Thus, most of the rainfall excess over the threshold value, which depends on the initial runoff rate, contributed to storm runoff as estimated in the previous studies (Tani et al., 1982; Tani and Abe, 1987a).

4.2. *Estimation of catchment area for SL*

The comparison of total storm runoff (m^3) between SL and MN for each storm event is given in Fig. 7(a). Enlarged plots for data close to the origin are shown in Fig. 7(b). For events with total storm runoff from MN smaller than about 160 m^3 (0.7 mm of water

Fig. 7. Comparison of total storm runoff between SL and MN. Symbols and storm numbers are the same as Fig. 5. (b) Enlarged plots for data close to the origin in (a).

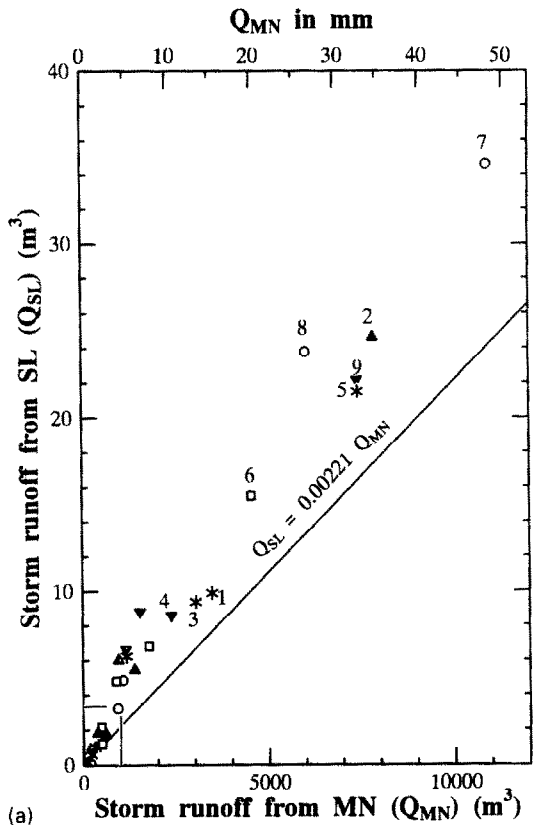
Q_{MN} in mm
0
10
20
30
40
50
Storm runoff from SL (Q_{SL}) (m^3)
0
10
20
30
40
Q_{SL} = 0.00221 Q_{MN}
1
2
3
4
5
6
7
8
9
0
5000
10000
Storm runoff from MN (Q_{MN}) (m^3)

(a)

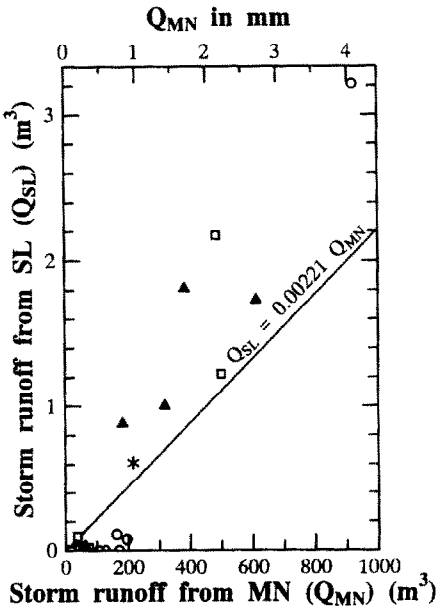
Q_{MN} in mm
0
1
2
3
4
Storm runoff from SL (Q_{SL}) (m^3)
0
1
2
3
Q_{SL} = 0.00221 Q_{MN}
0
200
400
600
800
1000
Storm runoff from MN (Q_{MN}) (m^3)

(b)

Table 1
Annual totals of rainfall and runoff yield in Tatsunokuchi-yama Experimental Forest from August 1 of 1986 to July 31 of 1987

	mm
Rainfall	874.5
Runoff yield	
SL	173.7
MN	169.9
KT	156.6

depth), runoff from SL is negligible. However, runoff from SL quickly increases when the runoff for MN is larger than 160 m^3. For large storm events, identified by numbers in Fig. 5, the rate increase in runoff from SL compared with MN becomes less.

These relationships may be attributed to differences in storm runoff generation processes between SL and MN. Total storm runoff from MN for each event consists of total storm runoffs from various kinds of slopes including SL. In some parts of catchment MN such as permanent wet zones near stream channels, stormflow is easily produced by a small amount of rainfall, whereas in areas with thick soils near the ridges of long slopes runoff is only produced after much rainfall. On the other hand, the rainfall amount needed to produce storm runoff must be in a narrower range for SL because of its short and steep slope, thin soil, and no distinct wet zone near channels. Absence of the wet zone must cause small amounts of storm runoff from SL for events when those from MN are smaller than 160 m^3. The steep increase in storm runoff from SL compared with that for MN (Fig. 7) may be attributed to a rapid extension of areas which contribute to storm runoff generation because of its topographic properties mentioned above. The rate of runoff increase from SL (relative to MN) becomes less for larger storms (see numbered data points). These more gently sloping lines may be related to data that show almost all the rainfall excess contributed to storm runoff in Fig. 5. This suggests that storm runoff was generated from the whole catchment area of MN including slope SL. Therefore, the gentle gradient in total storm runoff volume between MN and SL shown for large storm events in Fig. 7 may indicate the ratio of catchment area between them. Thus, the catchment ratio can be calculated as 0.00221 based on the gradient, and the catchment area for SL is estimated at 500 m^2 by multiplying the ratio by the catchment area of 22.61 ha for MN.

To assess this estimated value of catchment area of SL, we compare the annual total of runoff yield from SL with that from the entire catchments for the period from August 1 of 1986 to July 31 of 1987 (Table 1). Runoff yields from SL, MN, and KT are quite similar to each other. This supports the estimated catchment area of 500 m^2 for SL.

4.3. *Runoff development in a period of wetting transition*

Characteristics of hydrograph responses for SL can be now quantitatively compared with those for the entire catchments using runoff rates for a unit catchment area, since the catchment area of 500 m^2 has been fixed. A storm event (No. 7) was selected for our further analyses. The hydrographs are compared in Fig. 8(a). Event 7 was a long storm

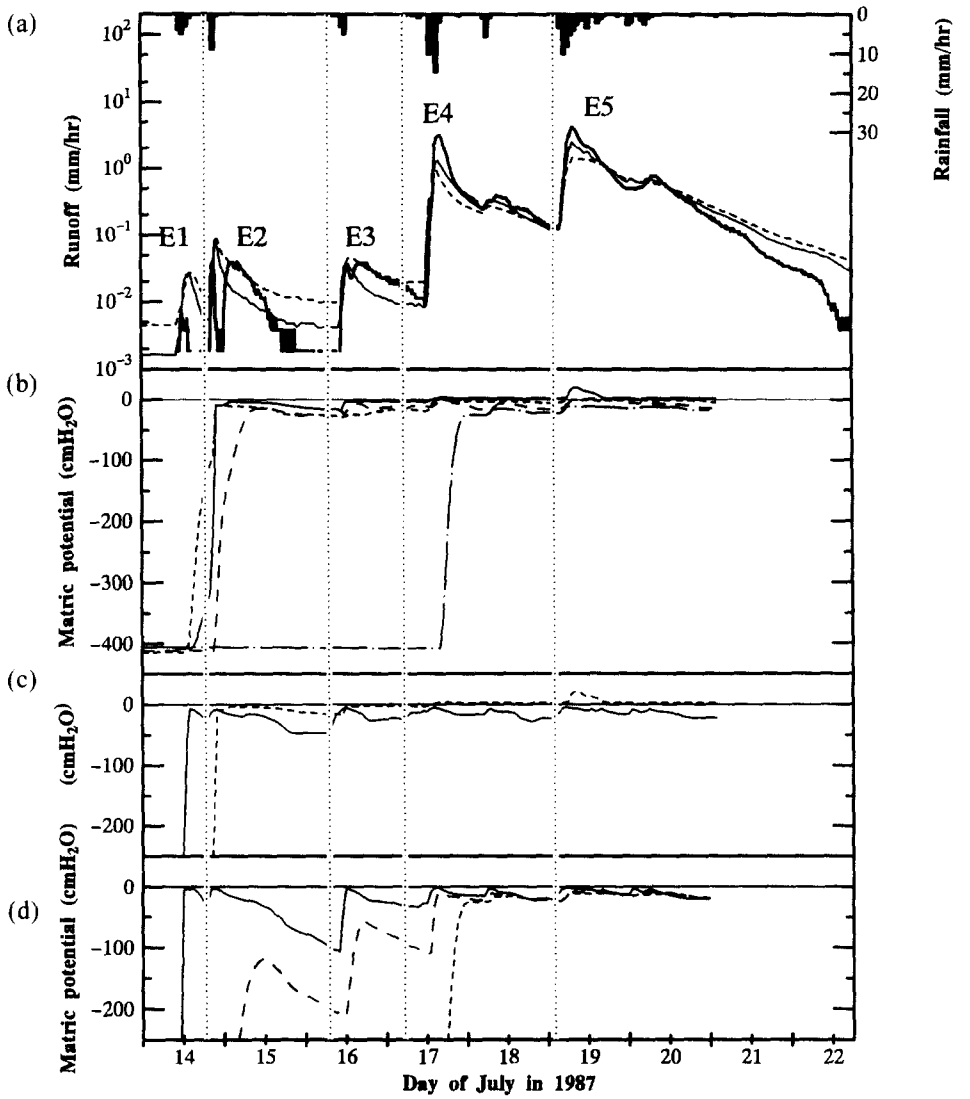

Fig. 8. Runoff responses and tensiometric responses for storm event No. 7. (a) Rainfall and runoff: ——, SL; - - -, MN; ——, KT. (b) Matric potential near bedrock: ——, T1; – – –, T2; - - -, T3; – - –, T4. (c) Matric potential at T1: ——, 10 cm; - - -, 46 cm. (d) Matric potential at T4: ——, 10 cm; – – –, 30 cm; - - -, 50 cm.

consisting of five episodes (E1–E5). The total amounts for rainfall and runoffs from SL, MN, and KT were 137.0, 69.1, 48.2, and 55.3 mm, respectively. The antecedent condition was dry, and the initial runoff rates for MN and KT were only 0.0046 and 0.0015 mm h^{-1}. The runoff amount and runoff ratio in each episode of the event for SL are listed in Table 2. To better understand these wetting transitions, tensiometric responses near bedrock at four sites (T1 to T4), responses at 10- and 46-cm depths in T1, and responses at 10-, 30-, and 50-cm depths in T4 are shown in Fig. 8(b), (c), and (d), respectively.

Table 2
Runoff response of SL in each episode within storm event No. 7

Episode	Duration	R_{ep}	R_{cu}	Q_{ep}	Q_{cu}	f_{ep}	f_{cu}
E1	10:40/14–18:40/14	13.0	13.0	0.015	0.015	0.001	0.001
E2	18:50/14–07:10/16	11.5	24.5	0.392	0.407	0.034	0.017
E3	07:20/16–05:20/17	9.5	34.0	0.486	0.893	0.051	0.026
E4	05:30/17–02:00/19	43.5	77.5	21.23	22.12	0.488	0.285
E5	02:10/19–18:00/22	59.5	137.0	47.00	69.12	0.790	0.505

R_{ep}, total rainfall in an episode; R_{cu}, cumulative rainfall; Q_{ep}, total runoff in an episode; Q_{cu}, cumulative runoff; f_{ep}, Q_{ep}/R_{ep}; f_{cu}, Q_{cu}/R_{cu}.

Fig. 9 shows a temporal change in relationship of cumulated runoff between SL and MN that is drawn on a background of Fig. 7. Boundaries between the episodes within the event are marked on the curve. This figure shows that this curve traces plots for the total runoff relationships in storm events: the cumulated runoff for SL was very small and less than that for MN during earlier episodes from E1 to E3. This increased rapidly and became larger than that for MN during E4. Finally, increasing rates of cumulated runoff for SL and MN were getting almost the same during E5. Thus, the sequence of runoff responses to this storm event may reflect general characteristics of storm runoff processes in our study

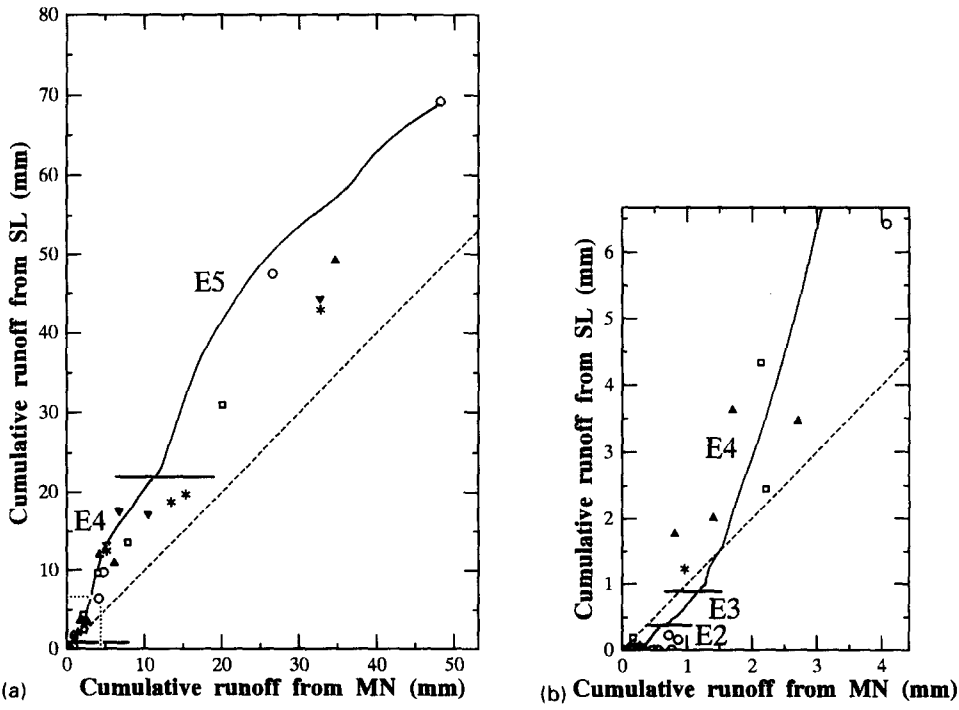

Fig. 9. A temporal change in relationship of cumulative runoff between SL and MN on a background of Fig. 7. (b) An enlarged view for the curve close to the origin in (a).

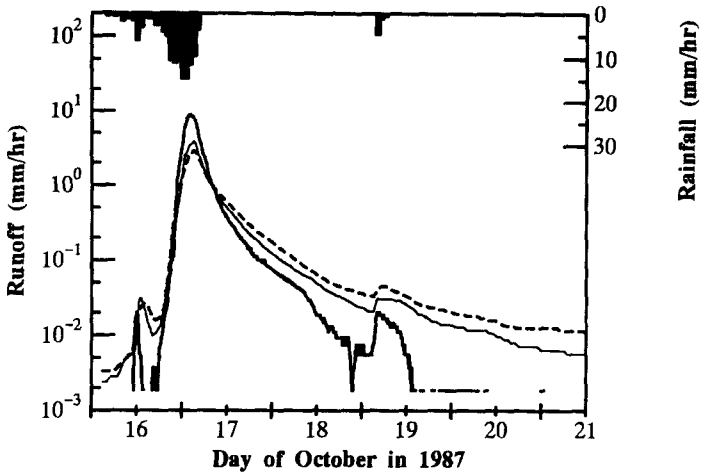

Fig. 10. Runoff responses for storm event No. 8. Symbols are the same as Fig. 8(a).

catchment and will give important information on storm runoff generation and its development during a period when the soil is accumulating moisture.

The relationships of cumulative runoff between SL and MN in this storm event may be divided into the earlier (E1 to E3) and the later episodes (E4 to E5). For the later episodes, as we have already estimated in Section 4.2, storm runoff was finally generated from the whole catchment area. Hydrographs were the steepest for SL, the second steepest for KT, and the gentlest for catchment MN (Fig. 8(a)). The same comparison results were obtained for other storms with large magnitudes. Hydrographs for storm Event 8 (October 16–18) are shown in Fig. 10 as an example. These results can be explained by the physical properties of each catchment. The steep hydrographs of SL may result from the thin soil layer, short and steep topographic properties, and the surface geology of quartz porphyry. Also in comparisons of hydrograph response between entire catchments MN and KT, steeper hydrographs for KT may be caused by steep slopes on the widespread quartz porphyry. Such an explanation based on the physical properties of each catchment may be attributed to the stable area for stormflow production which already extended to the whole catchment and did not change any more.

In the earlier episodes of Event 7 (E1 to E3), however, different types of responses consisting of short-lived and gentle hydrographs were produced for SL as shown in an enlarged figure (Fig. 11), although simple sharp hydrographs were formed for KT and MN. Detailed responses for SL were as follows: no response except for a short-lived response occurred during E1. A steep short-lived hydrograph response was followed by a gentle delayed response during each of E2 and E3. The two responses during E2 were separated, whereas those during E3 overlapped. These delayed responses for SL were rather behind the responses for MN and KT.

The volume of the short-lived response in SL during E1 was 0.015 mm and the ratio to the rainfall of 13.0 mm was about 0.1% (Table 2). The volume of the short-lived response during E2 was 0.045 mm and the ratio to the rainfall of 11.5 mm was about 0.4%. A short-lived response during E3 was also small though it overlapped with a larger delayed peak.

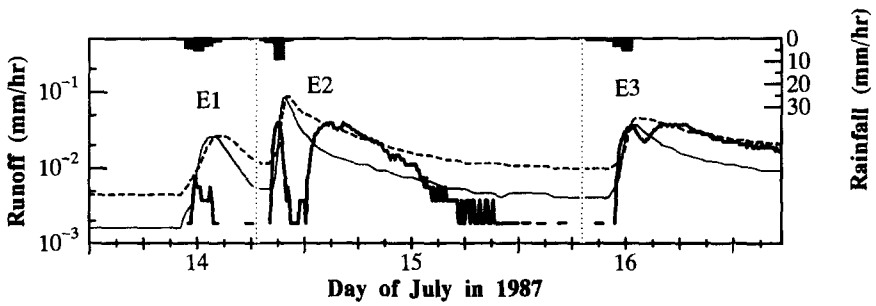

Fig. 11. An enlarged view of runoff responses for the earlier stage of storm event No. 7. Symbols are the same as Fig. 8(a).

The ratios of the short-lived response to the rainfall are very small and multiplying the catchment area of SL (500 m^2) by the ratio of 0.4% gives only an area of 2 m^2, which was similar to the area of the observation trench itself (length = 6 m, width = 0.5 m). Although this trench was covered with a roof and direct rainfall was not included in the runoff records, it is supposed that local lateral flow in the thin organic soil layer generally occurred on the mineral soil surface and might have directly entered the trench.

The delayed response first appeared during episode E2 with a large time-lag compared with the short-lived response (Fig. 11). During E3, however, the time-lag became small and the double peaks overlapped. Recession of the response for E3 was gentler than that for E2. As a result, the runoff ratio for E3 was larger than that for E2 though total rainfall for E3 was smaller than that for E2, as shown in Table 2. These results suggest that the contributing area for the delayed response was extending gradually even if the area remained still local.

Thus, those delayed responses from SL during the earlier episodes were different from those expected from comparisons of physical properties with the entire catchments. Wet zones near stream channels, which do not exist in the area of SL (Section 4.2), may involve differences of responses between SL and the entire catchments. However, no field evidence can be obtained for a runoff generation process for the catchments. For SL instead, we can refer to data on tensiometric responses next to make further considerations about runoff generation.

5. Tensiometric responses

5.1. Responses near surface

In this section, we will mainly discuss vertical propagation of the rainfall pulse based on tensiometric responses since it may be important for generation processes of lateral storm-flow. First we focus on responses of near-surface tensiometers monitored at 10-cm depths of T1 and T2. Matric potential values (ψ) at both sites approached zero at several times responding to rainfall peaks during the storm Event 7 as shown in Fig. 8(c) and (d). Fig. 12 shows the relationships of ψ at the 10-cm depth to the rainfall intensity (average for the 3-h period before peak) at each of the two sites. Although ψ values are different for T1 and T4,

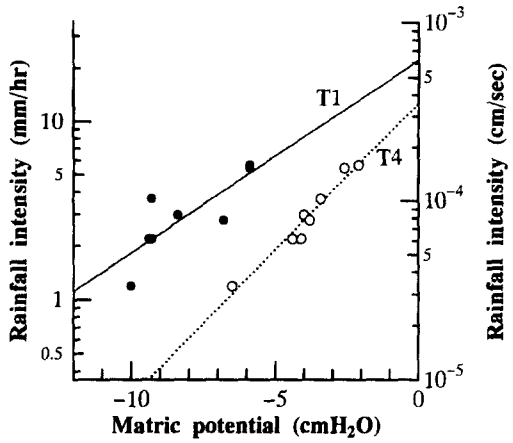

Fig. 12. Relationships of ψ at the 10-cm depth for T1 and T4 to rainfall intensity. The rainfall intensity is averaged for the 3-h period before peak. ●, T1; ○, T4.

they appear to decrease exponentially against the rainfall intensity. Rubin and Steinhardt (1963) theoretically demonstrated, based on applications of the Richards equation to vertical infiltration, that surface moisture content approaches a definite limit value giving the hydraulic conductivity the value of which is equal to the constant value of rainfall intensity, assuming the intensity is equal to or less than the saturated conductivity. Though the rainfall intensity was not constant for our case, the relationships in Fig. 12 suggest that each ψ value may indicate the definite limit value giving the hydraulic conductivity equal to the average of rainfall intensity. Thus, we can estimate that sequences of ψ at 10-cm depths of both sites reflected vertical flow within the soil matrix that should follow the Richards equation.

5.2. *Responses near bedrock*

Next we look at changes of matric potential near bedrock for T1, T2, T3, and T4 in Fig. 8(b). ψ for each of T1, T2, and T3 decreased to low values during episode E2, whereas ψ for T4 kept high negative values throughout the early stage of the storm event until it decreased during E4. Although changes in ψ at 10-cm depths of T1 and T4 were similar to each other, the response of ψ at 50 cm depth of T4 was very late compared with that at 46 cm depth of T1. Because the initial values of ψ were high in all of them, this difference was probably caused by different propagation of the rainfall pulse between those sites after the storm event started. A generation of vertical preferential flow may be involved in the difference and will be discussed more next.

5.3. *Possible generation of vertical flow through macropores*

Fig. 12 shows that both saturated hydraulic conductivities extrapolated from regression lines for the relationships at T1 and T4 are estimated at 3.6 and 6.3 $\times$ 10^{-4} cm s^{-1}, respectively. These values are much smaller than the values of saturated hydraulic

conductivity measured with the constant-head method, which were 1.7×10^{-3} cm s^{-1} and 6.3×10^{-3} cm s^{-1} (Section 2.2). This suggests that a discontinuous jump for the hydraulic conductivity may exist between full saturation and just below saturation. Large values of saturated hydraulic conductivity for full saturation must be due to flow within macropores (Watson and Luxmoore, 1986; Ohte et al., 1989). McDonnell (1990) emphasized distinguishing between the conductivity of the matrix and that of the soil with macropores, and he stated that local ponding which occurs when rainfall intensity is greater than the conductivity of the matrix will lead to vertical bypassing. In our field conditions, the extrapolated hydraulic conductivities for these sites coincide with the rainfall intensities of 12–23 mm h^{-1}, which were the only similar magnitudes to the observed rainfall intensities, and probable wide distribution ranges of both net rainfall under the forest canopy (stemflow also accelerates the concentration of rain water) and soil permeability must cause occurrences of local ponding as well as local lateral flow within the organic soil layer on the mineral soil surface. Evidence for them can be obtained from short-lived responses of runoff from SL in the early stage of our storm event (see Section 4.3). Thus, we may estimate a role of flow within macropores in the vertical quick propagation of the rainfall pulse. In this sense, it can be supposed that responses of matric potential near the bedrock at T1, T2, and T3, which decreased to low values earlier during E2, were controlled more by the larger contribution of quick flow within macropores than those at T4 that demonstrated the propagations with wetting front in Fig. 8(d).

5.4. *Vertical quick propagation through the soil matrix*

After ψ decreased to low values, changes of ψ were very small in all the tensiometer records and every response of ψ to rainfall became rapid even for records just near the bedrock, as shown in Fig. 8(b)–(d). ψ at 50 cm of T4, which was the last to decrease to low values, also shows quick responses during episode E5. Of course, it is rationale for vertical quick flow within macropores to pass rain water to deep soil near the bedrock (McDonnell, 1990). In wet conditions where ψ has low values throughout the soil as shown in ψ responses at 30 cm of T4, however, we should take into consideration that matrix flow also would contribute to a quick response of ψ just near the bedrock to a rainfall pulse. A general discussion based on the Richards equation may be necessary for this contribution.

Usually a capillary fringe effect has been widely accepted for the quick response driven by matric force (e.g. Novakowski and Gillham, 1988; Germann, 1990). In a more general sense, however, a strong nonlinearity in vertical infiltration under conditions of Darcian flow described by the Richards equation may be involved in the quickness of the pulse response (Kirkby, 1988). The Richards equation is described in a one-dimensional vertical form as:

$$C\frac{\partial\psi}{\partial t}=\frac{\partial}{\partial z}\left[K_c\left(\frac{\partial\psi}{\partial z}+1\right)\right] \tag{3}$$

where C is the specific moisture capacity ($=\mathrm{d}\theta/\mathrm{d}\psi$), K_c is the hydraulic conductivity, and z is the vertical co-ordinate axis. This equation shows a change of water storage capacity described as the left side controls the propagation of ψ. In a steady condition where the left side is equal to zero such as within the capillary fringe ($C = 0$), an input rainfall pulse

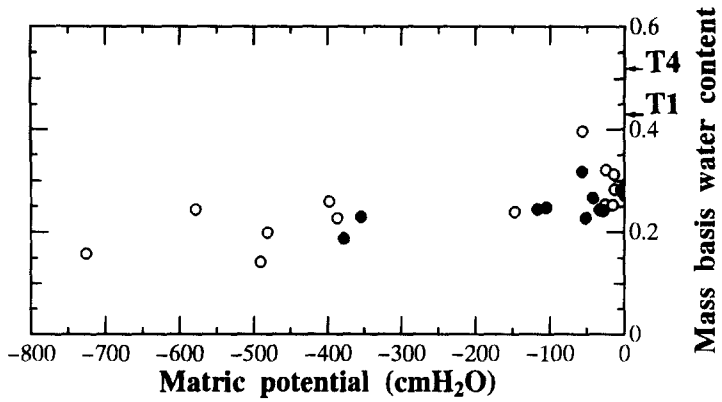

Fig. 13. Relationships between matric potential and mass-basis water content on the slope SL. ●, T1; ○, T4. The arrows indicate mass-basis water content at saturation (W_s).

would be propagated with the infinite celerity to the deep soil. On the other hand, when the water storage capacity can increase greatly from a dry initial condition, the pulse would be propagated with a slow celerity, making a wetting front. Therefore, the propagation depends on the change in water storage within the soil matrix responding to a rainfall pulse. Tani (1985a) showed, based on an application of the Richards equation to a homogeneous vertical soil column, that the rising of the groundwater table derived from a small amount of rainfall given to the surface was quite slow due to the redistribution process of water in soil, but also that this was much faster when a large amount of rainfall was given. According to a similar methodology, Tani (1985b) demonstrated that although the discharge from the bottom of a soil column increased very slowly in a dry period due to small rainfall inputs, it rapidly increased with greater input volumes even for a sandy soil with a small capillary fringe. These results suggest that a quick propagation of a rainfall pulse occurs in wet conditions established by large cumulative rainfall even when only water flow derived by matric force is considered.

In our case, once ψ decreases to low values throughout the vertical soil profile, temporal changes in ψ are small in range as shown in Fig. 8(b)–(d). Therefore, $\partial\psi/\partial t$ in Eq. (3) was continuously small. As for values of C in this equation, we should look at the water retention characteristics for our study site. Fig. 13 shows relationships between ψ and mass-basis water content (W) collected by a bore stick at the 10-cm depths of T1 and T4 (Section 2.2). Mass-basis water content at saturation (W_s) calculated from the porosity is indicated by an arrow for each site of T1 and T4. A wide scatter for the plots may be caused by a hysteresis in the relationships as well as spatial heterogeneities, but the following tendencies can be found for both T1 and T4: (1) mass-basis water content gradually increases with decreasing ψ; (2) W values just below $\psi = 0$ are much smaller than W_s; (3) no capillary fringe exists.

Because soil samples used here were collected by a bore stick and perfectly disturbed, it is believed that only the water within the soil matrix was measured as the value of W and that water within macropores was not included in W. Large differences in W between full saturation and just below saturation may be attributed to the existence of macropores, but

as far as water within the soil matrix is considered, an increase of water content with decreasing ψ is small in range. Thus, the left side of Eq. (3) was estimated small after the observed ψ decreased to low values, contributing to a quick propagation of rainfall pulse. Kosugi (1994) analyzed water retention curves for many kinds of soils and detected a large increase of water content just near saturation for typical forest soils. We can estimate that although capillary fringe for a forest soil is small in general, quick responses of ψ driven by matric forces may occur when ψ is low.

Accordingly, it can be suggested that flow within the soil matrix as well as macropore flow may also contribute to quick responses of ψ near bedrock under wet conditions of our storm event. Circumstantial evidence for this quick response within the matrix is shown in Section 4.3 where a large amount of rainfall (79%) contributed to storm runoff of SL in the last episode (E5) of Event (7) (Table 2). This runoff ratio would become large considering that the net rainfall given to the soil surface must be lower than the gross rainfall (see Section 6.2). It is unrealistic that such a high runoff ratio was derived from only macropore flow. Instead, the following is believed to be a more plausible runoff generation process: the surface soil layer in almost the entire slope area including T4 site was made wet at least during episode E5, and a 'cooperation' of both macropore and matrix flows contributed to stormflow.

6. Model application

6.1. Kinematic wave model and the effective rainfall

When a kinematic wave model was applied to a storm event for the entire catchment KT, the effective rainfall given to the lateral stormflow was estimated from the cumulative rainfall exceeding the initial threshold soil water deficit just before the storm event. The spatial distribution of the threshold deficit had to be empirically adjusted so that a good agreement between the observed and simulated hydrographs could be obtained (see Section 3.2) (Tani and Abe, 1987a). On the other hand, we can utilize responses of ψ to estimate the effective rainfall when we apply the model to runoff responses from the study slope SL. Thus, our aim in this chapter is to elucidate storm runoff processes there through incorporating conditions of matric potential at a point scale with runoff responses at a slope scale.

First, we presuppose that storm runoff from SL is produced by a lateral flow along the bedrock on the slope that is fast enough to contribute to storm runoff and can be described by a kinematic wave equation. Although the hydraulics and spatial distributions of this flow are both unknown, a system of saturated pipeflows may play a main role in this fast flow (McDonnell, 1990). For estimating effective rainfall given to the lateral flow, we define a propagation area where the effective rainfall is provided to the lateral flow through either macropore flow or matrix flow, and the propagation area and the other area are assumed to be clearly divided on the slope. Then, we can make the following assumptions based on the findings from Section 5.3: (1) a rainfall pulse is propagated from the soil surface to the bedrock through the soil layer without time-lag or attenuation and given to the lateral flow as an effective rainfall within a propagation area on the slope; (2) at the

outside of the propagation area, no rainfall is given to the lateral flow; (3) the establishment of propagation area is estimated from the condition of ψ just near the bedrock. Once this has decreased to −30 cm H_2O, this point is assumed to be included in the propagation area. This assumption has been adopted since the propagations of change in ψ from the 10-cm depth to the depth of near the bedrock, 46 cm for T1 or 50 cm for T4, appeared quick enough after ψ near the bedrock decreased to this value (Fig. 8(c) and (d)).

Therefore, the effective rainfall rates (i) for Eq. (2) within the propagation area and out of the area are, respectively, given as:

$$\begin{aligned} i &= 0 && \text{for } R < R_s \\ i &= r\cos\omega && \text{for } R \geq R_s \end{aligned} \tag{4}$$

where R is the cumulative rainfall integrated from the beginning of a storm event, and R_s is the threshold soil water deficit that is equal to cumulative rainfall integrated to the time when ψ just near the bedrock reaches −30 cm H_2O.

For our storm event, this condition was completed just after the rainfall during episode E2 for T1 and T3, several hours later during E2 for T2, and during the rainfall in E4 for T4. These results indicate that rainfall at latest from the beginning of episode E3 was given to the lateral flow at T1, T2, and T3, whereas only rainfall at and after the latter half of E4 was given to it at T4. The values of initial threshold soil water deficit for the former and the latter can be estimated at 24.5 mm and 70.0 mm from the cumulative rainfall. Based on this information, we make a further assumption that these two values represent the threshold deficit for downslope portions from the trench to T4 (the relative slope areas of 26%) and the deficit for upslope portions from T4 to the hilltop (the area of 74%), respectively. This assumption for the distributions of the initial threshold water deficit leads the extension of propagation area from the downslope portions of the slope at the beginning of E3 to the whole slope area at the latter half of E4.

6.2. *Net rainfall in forest*

Net rainfall in forest on the slope surface consisting of throughfall and stemflow has not been considered for estimating the effective rainfall because it was not observed for our study site. Here we consider effects of the net rainfall by referring to results from a similar forest. Iwatsubo and Tsutsumi (1967) studied observations in a natural mixed forest of deciduous and evergreen broad-leaved trees in Kamigamo Experimental Forest Station of Kyoto University in Kyoto, Japan. According to the observation results, the cumulative net rainfall (R_{net}) from the beginning of the event, which was the sum of the cumulative throughfall (T_f) and the cumulative stemflow (S_f), was calculated from the cumulative gross rainfall (R) by

$$\begin{aligned} R_{net} &= 0 && \text{for } R \leq 0.87 \\ R_{net} &= T_f = 0.589R - 0.51 && \text{for } 0.87 < R \leq 4.6 \\ R_{net} &= T_f + S_f = 0.853R - 1.72 && \text{for } R > 4.6 \end{aligned} \tag{5}$$

The intensity of net rainfall is given as dR_{net}/dt. Because the forest condition was poor for our slope SL, however, the actual net rainfall is believed to be larger than the value calculated by Eq. (5). Considering this point, we calculate hydrographs by the kinematic wave model from both of the gross rainfall (case G) and the net rainfall estimated by Eq. (5) (case N).

6.3. Simulation results

Hydrograph responses calculated for the two cases are shown in Fig. 14(a). Fig. 14(b) is attached to compare the details of hydrographs during the latter half of the event with a normal runoff scale instead of Fig. 14(a) with a logarithmic scale suitable for comparing the shapes of hydrographs with wide runoff ranges. In these simulations, the slope length was estimated at 51.9 m (calculated from the horizontal length of 42.7 m and the gradient of 34.6°). The shape of the slope area may be convergent because the trench length is only 6 m, but a rectangular catchment (width of 11.7 m calculated from the slope area of 500 m^2) was assumed for simplicity. The same values as were used for KT were assigned to parameters in Eq. (1): $p = 0.3$ and $k = 0.6\ m^{0.4}\ s^{0.3}$.

Fig. 14(a) and (b) give the following results: (1) no responses are calculated for episodes E1 and E2 because the cumulative rainfall does not exceed the threshold deficit value of 24.5 mm; (2) for episode E3, the calculated responses for the two cases show similar magnitudes to the observed response although the calculated hydrographs keep constant

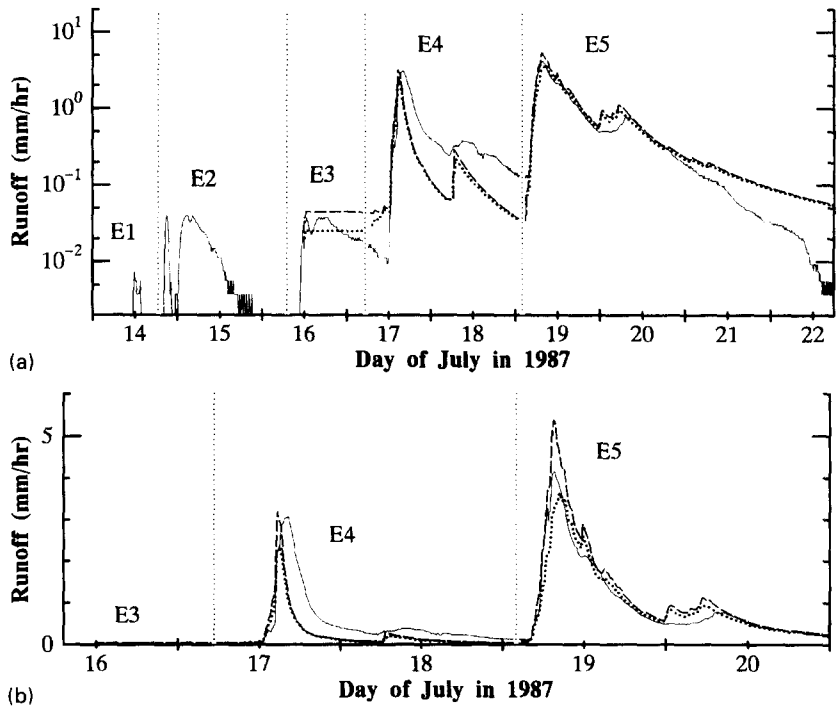

Fig. 14. Comparison between observed and simulated hydrographs for storm event No. 7. (a) With a logarithmic scale. (b) With a normal scale. ——, Observed; - - -, simulated for case G; · · ·, simulated for case N.

values during the recession stage of the observed hydrograph; (3) the calculated responses during episode E4 are smaller than the observed response; (4) good agreements are obtained for responses during episode E5, the final stage of the storm event. Detailed discussion for runoff generation processes will be made next in the reverse order from episode E5 because they may be estimated the simplest in the final wettest condition.

6.4. Estimation of runoff generation processes

During episode E5, the peak of observed response lies between peaks of responses calculated from case G and case N (Fig. 14(b)). However, the peak calculated based on the actual rainfall would be rather close to the observed peak since it is given to the soil surface on SL through its poor forest condition and probably estimated smaller than rainfall for case G and larger than that for case N. The generation area for the lateral flow was consistent with the whole slope area throughout this episode in our model simulation because the cumulative rainfall had exceeded the threshold soil water deficit everywhere on it before the starting of episode E5. Therefore, we can accept the assumptions that a lateral flow described by the kinematic wave equation produces a storm runoff from SL at least in the wettest condition of the storm event and that a rainfall pulse is propagated through the soil layer without time-lag and attenuation and given to the lateral flow within the propagation area defined in Section 6.1.

During episode E4, the calculated hydrographs even for case G underestimated the observed hydrograph. This means effective runoff was too small. Based on ψ response just near the bedrock of T4, we assumed that rainfall before the latter half of E4 was not given to the lateral flow on the upslope portions (74%) of SL. The underestimation suggests that ψ decreased earlier at some areas of these portions than ψ at T4 and that an earlier extension of the propagation area caused a larger production of the lateral flow.

In the early stage of the storm event, the calculated hydrograph keeps a constant runoff rate during E3 (Fig. 14(a)). This constant rate can be explained by the characteristics of kinematic waves in Eq. (2): this rate responds to the integration of rainfall given to the limited propagation area (the lower portions of 26%) during E3 since the duration of rainfall was shorter than the time when the characteristics of Eq. (2) starting at the upslope end of the propagation area reached the downslope end. Thus, the constant runoff rate (q_c) can be written as:

$$q_c = \left(\frac{R_{E3} \cos \omega}{k} \right)^{\frac{1}{p}} \tag{6}$$

where R_{E3} is the cumulative gross rainfall for case G or net rainfall for case N given to the lateral flow during E3. q_c values for G and N are calculated at 0.044 and 0.026 mm h^{-1}, respectively. However, these constant rates were derived only from an idealized lateral flow pathway and some runoff recession may be expected within the actual pathway after the rainfall ceased. In this sense, it is rather notable that the delayed peak of the observed response kept constant for about 4 h and the recession of observed runoff was gentler than any other recession in the storm event. In addition, the magnitude of calculated runoff response was similar to that of the observed response. These moderate comparison results

suggest that the response during E3 was derived from the same lateral flow as the flow producing the responses during E4 and E5 though the generation area for this lateral flow occupied only the lower 26% portions of SL during E3.

During E1 and E2, no calculated response appeared. Indeed no observed response appeared except for a short-lived response that was probably produced by local lateral flow on the mineral soil during E1 (see Section 4.3). During E2, however, a delayed response, a similar magnitude to that during E3, appeared after the short-lived response. This suggests that the lateral flow producing responses during episodes from E3 to E5 had been already active during E2. Therefore, we may estimate that within some part of the lower portions, ψ decreased earlier than ψ just near the bedrock at T1 and T3 and that the lateral flow had already appeared locally during E2.

Accordingly, we can conclude that the generation area of the lateral flow was extended from the lower portions to the whole slope as the cumulative rainfall became large and that the decreasing of matric potential near bedrock indicated its extension. However, no response calculated during E2 and an underestimated hydrograph during E4 showed that the generation area was extended somewhat earlier than expected from the records of four tensiometers. The following reasons may be involved in this quick expansion: the

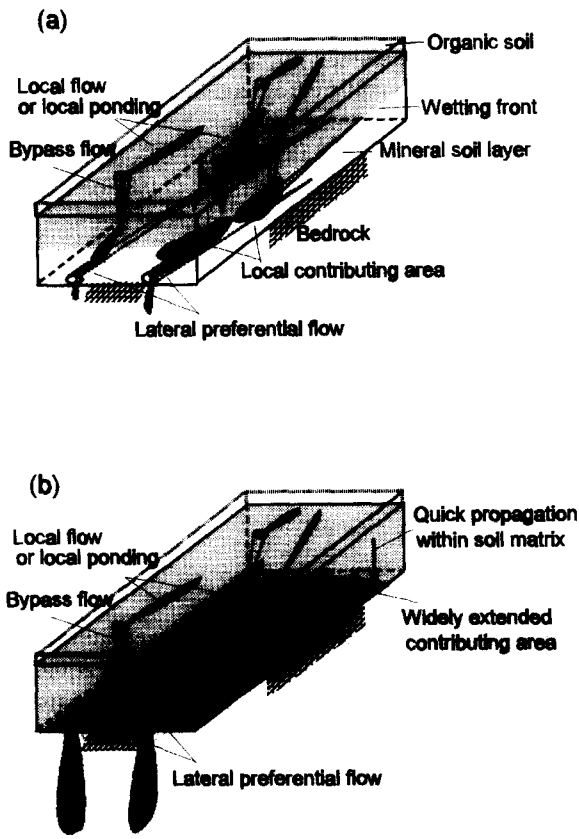

Fig. 15. Schematic representation of runoff generation. (a) A wetting transition. (b) The wettest condition.

thickness of the soil layer is small in some areas and bedrock is exposed at the head wall of the landslide (see Section 2.2). Bypass flow within macropores played an important role in the propagation of the rainfall pulse to the bedrock.

6.5. A schematic representation of runoff generation

Schematic representation of runoff generation processes in a transition from dry to wet conditions for a unit slope estimated in this paper can be illustrated by Fig. 15. Assume rainfall is given to the slope with a dry antecedent condition. Although most of the rain water was generally retained within the soil matrix making a wetting front, vertical bypass flow within macropores transports some rain water to deep soil near the bedrock due to generations of local ponding and/or local lateral flow within the organic soil layer in some portions of the surface of mineral soil. Quick lateral flow occurs through preferential pathways mainly consisting of pipes on the bedrock, and the flow derived from downslope portions reaches the downslope end. A small hydrograph response is produced by these processes (Fig. 15(a)).

As rainfall continues, matric potential near the bedrock decreases to a low value on large portions of the slope. Then, the lateral flows on the bedrock are connected with each other, and the contributing area for the storm runoff is extended finally to the whole slope area. Thus, a large runoff response is produced from the developed lateral flow receiving a rainfall pulse propagated quickly through both macropores and the soil matrix everywhere on the slope (Fig. 15(b)). This process ensures that most of the rainfall on the slope surface contributes to storm runoff.

7. Conclusion

Runoff generation processes have been estimated from hydrological observations conducted on a steep forested hillslope with a thin soil layer. Hydrological information obtained from previous studies for the entire catchments were utilized for the estimations as a clue. The most important information was that almost all the rainfall contributes to storm runoff when the soil condition is the wettest. This means the contributing area for storm runoff is stable, and that runoff generation process could be regarded as a transition from dry conditions to the wettest goal. Tensiometric responses obtained from the observations on the study slope demonstrated the basic roles of the mineral soil layer in vertical propagation of the rainfall pulse to deep soil. Application of a kinematic wave runoff model showed that quick lateral flow receiving quick propagation of the rainfall pulse produces storm runoff responses in the wettest condition and that a development of the same runoff processes occurs in the transition process from dry conditions.

Acknowledgements

I thank Dr Roy C. Sidle of the Geological Survey of Denmark and Greenland (now at Land–Ocean Interactions in the Coastal Zone (LOICZ) Project Office) for his valuable

comments. Construction of the trench system and maintenance of the hydrological observation system in the Tatsunokuchi-yama Experimental Forest were carried out by Muneyasu Matsuda, Mitsuharu Ohtaki, Chuichi Kobayashi, Hideko Shimamura, Shigeaki Hattori (now at Nagoya University), Toshio Abe, Yoshiaki Goto, and Koji Tamai at Kansai Research Center of Forestry and Forest Products Research Institute. Their contributions are gratefully acknowledged.

References

Abe, T., Tani, M., 1985. Streamflow changes after killing of pine trees by the pine-wood nematode. J. Jpn. For. Soc. 67, 261–270 (in Japanese with English abstract).

Betson, R.P., Aris, Jr., C.V., 1978. Implications for modelling surface-water hydrology. In: Kirkby, M.J. (Ed.), Hillslope Hydrology. John Wiley, Chichester, pp. 295–323.

Beven, K., 1981. Kinematic subsurface stormflow. Water Resour. Res. 17, 1419–1424.

Beven, K., Wood, E., 1983. Catchment geomorphology and the dynamics of runoff contributing areas. J. Hydrol. 65, 139–158.

Dunne, T., Black, R.D., 1970. An experimental investigation of runoff production in permeable soils. Water Resour. Res. 6, 478–490.

Freeze, A., 1971. Three-dimensional, transient, saturated–unsaturated flow in a groundwater basin. Water Resour. Res. 7, 347–366.

Fujieda, M., Abe, T., 1982. Effects of regrowth and afforestation on streamflow on Tatsunokuchiyama experimental watershed. Bull. For. For. Prod. Res. Inst. 317, For. For. Prod. Res. Inst., Tsukuba, pp. 113–138 (in Japanese with English abstract).

Germann, P., 1990. Macropores and hydrologic hillslope processes. In: Anderson, M.G., Burt, T.P. (Eds.), Process Studies in Hydrology. John Wiley, Chichester, pp. 327–363.

Hewlett, J.D., Hibbert, A.R., 1963. Moisture and energy conditions within a sloping soil mass during drainage. J. Geophys. Res. 68, 1081–1087.

Ishihara, T., Takasao, T., 1963. A study on runoff pattern and its characteristics. Disaster Prevention Research Institute Kyoto University Bulletin No. 65, Kyoto University, Kyoto, pp 23.

Iwatsubo, G., Tsutsumi, T., 1967. On the amount of plant nutrients supplied to the ground by rainwater in adjacent open plot and forests (2). Bull. Kyoto Univ. For. 38, 110–124 (in Japanese with English abstract).

Kidachi, M., Kishioka, T., Kobayashi, T., Abe, T., 1977. Analysis of the aquifer by electrical resistivity protecting in Tatsunokuchiyama Experimental Forest. In: Japanese Forestry Society (Ed.) Transactions of the 88th Annual Meeting of the Japanese Forestry Society, Tokyo. pp. 387–389 (in Japanese).

Kirkby, M.J. (Ed.), 1978. Hillslope Hydrology. John Wiley, Chichester, pp. 389.

Kirkby, M.J., 1988. Hillslope runoff processes and models. J. Hydrol. 100, 315–339.

Kitahara, H., 1993. Characteristics of pipe flow in forested slopes. In: Bolle, H.J., Feddes, R.A. and Kalma, J.D. (Eds), Exchange Processes at the Land Surface for a Range of Space and Time Scales. Proc. Yokohama Symp., IAHS Publ. No. 212. IAHS, Wallingford, pp. 235–242.

Kosugi, K., 1994. Three-parameter lognormal distribution model for soil water retention. Water Resour. Res. 30, 891–901.

Kubota, J., Sivapalan, M., 1995. Towards a catchment-scale model of subsurface runoff generation based on synthesis of small-scale process-based modelling and field studies. Hydrol. Processes 9, 541–554.

Linsley, R.K., Kohler, M.A., Paulhus, J.L.H., 1949. Applied Hydrology. McGraw-Hill, New York, 689 pp.

McDonnell, J.J., 1990. A rationale for old water discharge through macropores in a steep, humid catchment. Water Resour. Res. 26, 2821–2832.

Mosley, M.P., 1979. Streamflow generation in a forested watershed, New Zealand. Water Resour. Res. 15, 795–806.

Nakano, H., 1967. Effects of changes of forest conditions on water yield, peak flow and direct runoff of small watersheds in Japan. In: Sopper, W.E. and Lull, W.E. (Eds), Int. Symp. Forest Hydrology. Pergamon Press, New York, pp. 551–564.

Novakowski, K.S., Gillham, R., 1988. Field investigations of the nature of water-table response to precipitation in shallow water-table environments. J. Hydrol. 97, 23–32.

Ohte, N., Suzuki, M., Kubota, J., 1989. Hydraulic properties of forest soils, 1, The vertical distribution of saturated–unsaturated hydraulic conductivity. J. Jpn. For. Soc. 71, 137–147 (in Japanese with English abstract).

Rubin, J., Steinhardt, R., 1963. Soil water relations during rain infiltration, 1, Theory. Soil Sci. Soc. Am. Proc. 27, 246–251.

Sidle, R.C., Tsuboyama, Y., Noguchi, S., Hosoda, I., Fujieda, M., Shimizu, T., 1995. Seasonal hydrologic response at a various spatial scales in a small forested catchment, Hitachi Ohta, Japan. J. Hydrol. 168, 227–250.

Sklash, M.G., Farvolden, R.N., 1979. The role of groundwater in storm runoff. J. Hydrol. 43, 45–65.

Sklash, M.G., Stewart, M.K., Pearce, A.J., 1986. Storm runoff generation in humid headwater catchments, 2, A case study of hillslope and low-order stream response. Water Resour. Res. 22, 1273–1282.

Sloan, P.G., Moore, I.D., 1984. Modeling subsurface stormflow on steeply sloping forested watersheds. Water Resour. Res. 20, 1815–1822.

Tani, M., 1985a. The effects of soil physical properties on the groundwater-table rise. In: Takei A. (Ed.), Proc. Int. Symp. on Erosion, Debris Flow and Disaster Prevention. The Erosion-Control Engineering Society, Japan, Tokyo, pp. 361–365.

Tani, M., 1985b. Analysis of one-dimensional, vertical, unsaturated flow in consideration of runoff properties of a mountainous watershed. J. Jpn. For. Soc. 67, 449–460 (in Japanese with English abstract).

Tani, M., Abe, T., 1987a. Analysis of stormflow and its source area expansion through a simple kinematic wave equation. In: Swanson, R.H., Bernier, P.Y. and Woodard, P.D. (Eds), Forest Hydrology and Watershed Management, Proc. Vancouver Symp., IAHS Publ. No. 167. IAHS, Wallingford, pp. 609–615.

Tani, M., Abe, T., 1987b. An evaluation of the effects of forest change on streamflow using a runoff model. Bull. For. For. Prod. Res. Inst. 342, 41–60 (in Japanese with English abstract).

Tani, M., Abe, T., Kishioka, T., 1982. Runoff analysis on the condition that the whole rainfall is considered to be directed as storm runoff. In: Japanese Forestry Society (Ed.), Transactions of the 93rd Annual Meeting of the Japanese Forestry Society, Tokyo, pp. 463–466 (in Japanese).

Tsuboyama, Y., Sidle, R.C., Noguchi, S., Hosoda, I., 1994. Flow and solute transport through the soil matrix and macropores of a hillslope segment. Water Resour. Res. 30, 879–890.

Watson, K.W., Luxmoore, R.J., 1986. Estimating macroporosity in a forest watershed by use of a tension infiltrometer. Soil. Sci. Soc. Am. J. 50, 578–582.